Cellular/Molecular

Chloride Accumulation in Mammalian Olfactory Sensory Neurons

Hiroshi Kaneko, Ilva Putzier, Stephan Frings, U. Benjamin Kaupp, and Thomas Gensch
Institute for Biological Information Processing (IBI-1), Forschungszentrum Jülich, 52425 Jülich, Germany

The generation of an excitatory receptor current in mammalian olfactory sensory neurons (OSNs) involves the sequential activation of two distinct types of ion channels: cAMP-gated Ca^{2+}-permeable cation channels and Ca^{2+}-gated Cl^- channels, which conduct a depolarizing Cl^- efflux. This unusual transduction mechanism requires an outward-directed driving force for Cl^-, established by active accumulation of Cl^- within the lumen of the sensory cilia. We used two-photon fluorescence lifetime imaging microscopy of the Cl^--sensitive dye 6-methoxy-quinolyl acetoethyl ester to measure the intracellular Cl^- concentration in dendritic knobs of OSNs from mice and rats. We found a uniform intracellular Cl^- concentration in the range of 40–50 mM, which is indicative of active Cl^- accumulation. Functional assays and PCR experiments revealed that NKCC1-mediated Cl^- uptake through the apical membrane counteracts Cl^- depletion in the sensory cilia, and thus maintains the responsiveness of OSNs to odor stimulation. To permit Cl^- accumulation, OSNs avoid the "chloride switch": they do not express KCC2, the main Cl^- extrusion cotransporter operating in neurons of the adult CNS. Cl^- accumulation provides OSNs with the driving force for the depolarizing Cl^- current that is the basis of the low-noise receptor current in these neurons.

Key words: **olfaction; calcium-activated chloride channels; fluorescence lifetime imaging; chloride homeostasis; sensory transduction; chloride cotransport**

Introduction

Signal transduction in olfactory sensory neurons (OSNs) of mammals involves an unusual mechanism of current amplification that is based on the concerted action of two types of transduction channels: cAMP-gated cation channels and Ca^{2+}-gated Cl^- channels. Both channels are located in the plasma membrane of chemosensory cilia. The cilia are embedded in a thin mucus layer that forms an aqueous interface between the nasal cavity and the sensory epithelium (Fig. 1*A*). The mucus dissolves airborne odorants and mediates their interaction with the ciliary membrane (Getchell et al., 1984). Olfactory signal transduction begins when odorants bind to receptor proteins and trigger the synthesis of the second messenger cAMP (Buck, 2000; Frings, 2001). When the ciliary cAMP concentration reaches micromolar levels, cAMP-gated cation channels open and Ca^{2+} and monovalent cations flow from the mucus into the ciliary lumen (Leinders-Zufall et al., 1998; Dzeja et al., 1999). The primary depolarizing cation current is then boosted ~10-fold by Ca^{2+}-induced Cl^- efflux from cilia to the mucus, thus generating a receptor current that leads to electrical excitation of the OSN (Kleene, 1993; Kurahashi and Yau, 1993; Lowe and Gold, 1993). This Cl^--based amplification mechanism (Fig. 1*B*) appears to be unique to OSNs and is understood to serve an important purpose for the OSNs: high-gain, low-noise current amplification (Kleene, 1997; Reisert et al., 2003). The basis of the high gain seems to be an eightfold excess of Ca^{2+}-gated Cl^- channels over cAMP-gated cation channels, whereas noise reduction results from averaging of local Ca^{2+} signals at the cytosolic side of the ciliary membrane (Reisert et al., 2003).

A unique feature of this transduction process is that OSNs, unlike other primary neurons, need an unusually high intracellular Cl^- concentration, $[Cl^-]_i$, to drive the Cl^- flux in the outward direction. Active accumulation of Cl^- against an electrochemical gradient is required to prime OSNs for the generation of a Cl^--based receptor current. In this regard, OSNs differ fundamentally from neurons of the CNS, which keep $[Cl^-]_i$ low (<10 mM), because the action of inhibitory synapses in the CNS depends on Cl^- influx. Therefore, in contrast to CNS neurons, Cl^- transport and Cl^- homeostasis in OSNs must be organized in such a way that it promotes Cl^- accumulation instead of Cl^- extrusion. Furthermore, steady-state modeling has demonstrated that Ca^{2+}-dependent Cl^- efflux during odor detection would rapidly deplete the small ciliary lumen of Cl^- unless an efficient Cl^- accumulation mechanism counteracts the Cl^- loss and stabilizes $[Cl^-]_i$ (Lindemann, 2001).

Although $[Cl^-]_i$ plays such a central role in olfactory transduction, little information about Cl^- homeostasis in OSNs is available to date. Two previous studies indicate a range for $[Cl^-]_i$ of 20–80 mM. However, these data were obtained from isolated

Received June 1, 2004; revised July 1, 2004; accepted July 18, 2004.

This work was supported by the Deutsche Forschungsgemeinschaft under Grants SPP 1025 (I.P.) and FOR 450/1 (H.K.). We thank Dr. Joseph Lynch for valuable comments on this manuscript.

Correspondence should be addressed to Prof. Stephan Frings, Department of Molecular Physiology, Im Neuenheimer Feld 230, 69120 Heidelberg, Germany. E-mail: s.frings@zoo.uni-heidelberg.de.

H. Kaneko's and S. Frings's present address: Department of Molecular Physiology, University of Heidelberg, Im Neuenheimer Feld 230, 69120 Heidelberg, Germany.

I. Putzier's present address: Department of Cell Biology, Emory University School of Medicine, 615 Michael Street, Atlanta, GA 30322.

DOI:10.1523/JNEUROSCI.2115-04.2004

 0270-6474/04/247931-08$15.00/0

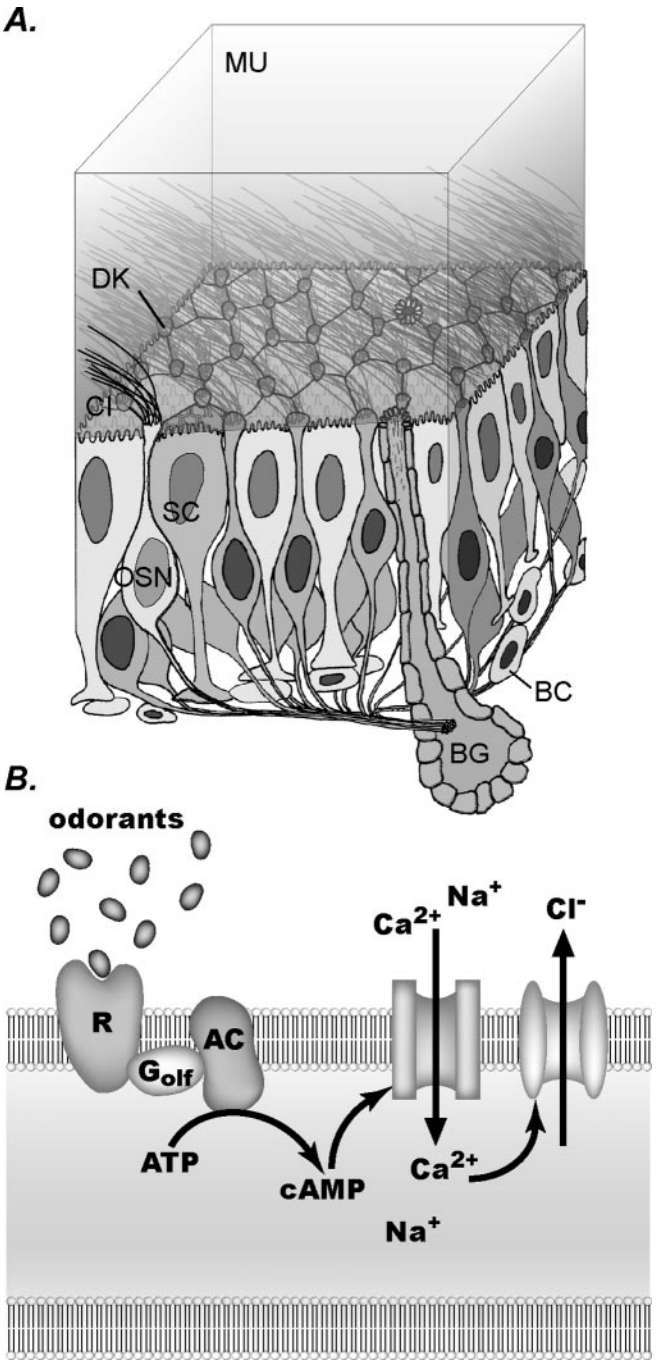

Figure 1. Olfactory signal transduction. *A*, Schematic drawing of the olfactory neuroepithelium. The epithelial surface is covered with mucus (MU) that forms the environment for the chemosensory cilia (Cl) of OSNs. Epithelial supporting cells (SC) form the apical surface and maintain a regular pattern of dendritic knobs (DK), the apical endings of OSN dendrites. Basal cells (BC) are nondifferentiated neurons that continuously replace OSNs. The mucus layer is primarily supplied by Bowman's glands (BG). *B*, The current model of excitatory components in olfactory signal transduction. Odorants bind to olfactory receptor proteins (R), which induce activation of type III adenylyl cyclase (AC) through the G-protein G_{olf}. cAMP opens cyclic nucleotide-gated ion channel, leading to Ca^{2+} influx and activation of Ca^{2+}-gated Cl^- channels.

rat OSNs (Kaneko et al., 2001) and from cryosections of rat olfactory epithelium (Reuter et al., 1998), respectively. $[Cl^-]_i$ measurements from living OSNs in intact epithelium have not proved possible so far. Here, we apply a novel method [two-photon fluorescence lifetime imaging microscopy (2P-FLIM)] that allows both the determination of $[Cl^-]_i$ in the dendritic endings of intact, viable OSNs, and the investigation of the local Cl^--transport mechanism involved in Cl^- homeostasis.

Materials and Methods

Tissue preparation. Rats and mice (6–8 weeks of age) were killed with 1.0–1.5 ml isoflurane. The nasal cavity was opened along a septum so that olfactory turbinates were exposed. Turbinates were removed from the nasal cavity and soaked in extracellular solution. The olfactory epithelium was detached from the turbinates without damaging the tissue surface. For cell isolation, the epithelium was cut into ~1 mm^2 pieces and treated in low-divalent ion solution with 0.1% trypsin for 10 min at room temperature. After trypsinization, the cell suspension was triturated with a Pasteur pipette in extracellular solution containing 0.05% DNase I. Intact olfactory epithelium or isolated cells were incubated in extracellular solution containing 5 mM 6-methoxy-quinolyl acetoethyl ester (MQAE) (Molecular Probes, Eugene, OR) for at least 1 hr (isolated cell) or 1.5 hr (intact epithelium) at room temperature in the dark. The dye progressively accumulates within cells as the molecule is rendered membrane impermeable by cytosolic esterases (Koncz and Daugirdas, 1994) with only little effect on its fluorescence properties (Kaneko et al., 2002). Isolated cells loaded with MQAE were fixed on a cover glass coated with Cell-Tak (BD Biosciences, Mountain View, CA). For 2P-FLIM experiments, the cover glass was placed in a bath chamber that was equipped for solution exchange. MQAE-loaded pieces of epithelium were placed in a drop of extracellular solution on an acryl plate and immobilized with 1 cm^2 nylon mesh (Monodur PA150N). To hold the epithelium in place, the nylon mesh was sandwiched between the acryl plate and a silicone disc with a cone-shaped aperture (opening diameter, 3 mm). The tissue was mounted inside a bath chamber where the solution could be exchanged in <1 min. All of the recordings were done at room temperature (295 K).

2P-FLIM measurements. MQAE was used as a fluorescent probe for intracellular Cl^- (Verkman, 1990). MQAE molecules reach the excited state on absorption of a single ultraviolet photon (λ = 375 nm) or, alternatively, the simultaneous absorption of two infrared photons (λ = 750 nm). We used two-photon excitation to achieve an optical resolution of ~0.5 μm and 1 μm in the plane of the epithelial surface (x- and y-axes) and perpendicular to the surface (z-axis), respectively. Moreover, the infrared light used for two-photon excitation caused no detectable photodamage, even with the relatively long observation times of up to 10 images with 1 min of illumination per image. UV light needed for one-photon excitation is expected to cause considerable photodamage if used for such long times with the required intensities. In the MQAE molecule, the dwell time in the excited singlet state (the fluorescence lifetime, τ) is near 30 nsec in water containing 50 μM MQAE and is reduced by anions through collisional quenching. The Cl^- dependence of τ is described by the Stern–Volmer relation ($\tau_0/\tau = 1 + K_{SV}[Cl^-]$), where τ_0 is the fluorescence lifetime in 0 Cl^-, and K_{SV}, the Stern–Volmer constant, is a measure of the Cl^- sensitivity of MQAE. K_{SV} has a value of 185 M^{-1} in water but only 5–20 M^{-1} inside cells. This reduced sensitivity of intracellular MQAE probably results in part from interactions of the dye with other soluble anions (in particular, HPO_4^{2-} and HCO_3^-) and from self-quenching of MQAE at concentrations >100 μM (Kaneko et al., 2002).

For 2P-FLIM measurements, the tissue sample was placed on the stage of an upright fluorescence microscope (BX50WI; Olympus Optical, Tokyo, Japan) and observed through a 60× water-immersion objective (numerical aperture, 0.9; Olympus Optical). Fluorescence was excited with 150 fsec light pulses (λ = 750 nm) applied at sufficient intensity to generate two-photon excitation. Light pulses were generated at a frequency of 75 MHz by a mode-locked Titan-Sapphire laser (Mira 900; output power, >500 mW; Coherent, Santa Clara, CA), which was pumped by the frequency-doubled output (532 nm) of a Nd–vanadate laser (Verdi; Coherent). The laser light was directed through the objective to the epithelial surface at reduced power (2.5 mW) using a beam scanner (TILL Photonics, Munich, Germany). Fluorescence was recorded by photomultipliers, and lifetime analysis was performed using

electronics (SPC-730; Becker & Hickl, Berlin, Germany) and software (SPC7.22; Becker & Hickl) for time-correlated single-photon counting (Lakowicz, 1999). Lifetime images were analyzed using SPCImage 1.8 and 2.6 (Becker & Hickl) and ImageJ (National Institutes of Health). A detailed description of the instrument and the calibration procedure was published by Kaneko et al. (2002). Images were obtained by scanning the excitation light focus over the apical epithelial surface or, in some experiments, through deeper layers of the epithelium. Mean values of lifetimes and Cl^- concentrations are given as ±SDs.

Identification of Cl^- cotransporter genes. To identify genes encoding chloride transporters in OSNs, PCR was performed on cDNA from rat olfactory epithelium and, for controls, on cDNA from rat kidney, cerebellum, or hippocampus. Primers were designed against conserved regions (transmembrane domains) of each protein. The primers were specific for subtypes of cotransporters and were designed to span several exons: KCC1, 719 bp (1245–1964); KCC2, 645 bp (1286–1931); NKCC1, 685 bp (1676–2361); NKCC2, 718 bp (1222–1940); NCC, 713 bp (1373–2086). The resulting PCR products were cloned into pBluescript SK^- and sequenced.

Results

Surface-scan 2P-FLIM of olfactory epithelium

The use of two-photon excitation for scanning fluorescence microscopy provides a three-dimensional resolution that is limited only by the size of the laser focus used for excitation. With optical sectioning at a resolution of 1 μm, structures near the surface of the olfactory epithelium, in particular dendritic knobs, distal dendrites, and supporting cells, can be optically resolved (Denk and Svoboda, 1997). To determine $[Cl^-]_i$ in OSNs, we loaded the cells with the fluorescent Cl^- indicator MQAE. Cl^- ions interact with this dye in the excited state and reduce fluorescence intensity and fluorescence lifetime by collisional quenching (Verkman, 1990; Lakowicz, 1999). MQAE has been recently used for Cl^- detection in isolated OSNs (Kaneko et al., 2001), dorsal root ganglion neurons (Kaneko et al., 2002), frog taste disks (Li and Lindemann, 2003), and brain slices (Marandi et al., 2002). Provided the quenching efficiency inside the olfactory neuron is known (see next paragraph) (see Fig. 3*B*), the fluorescence lifetime analysis yields absolute values for $[Cl^-]_i$ independent of the local cytosolic dye concentration (Kaneko et al., 2002). Fluorescence lifetime signals from cytosolic MQAE, elicited by two-photon excitation and recorded near the apical surface of the olfactory epithelium, revealed a striking difference in the lifetime between dendritic knobs and supporting cells (Fig. 2*A*). In normal extracellular solution ($[Cl^-]$ = 150 mM), we measured a mean lifetime τ in supporting cells of 3.2 ± 0.1 nsec (nine supporting cells in three epithelia), and a significantly lower value in dendritic knobs (τ = 2.5 ± 0.2 nsec; nine knobs in three epithelia). This indicates a significant difference in $[Cl^-]_i$, with the dendritic knobs having the higher values. To obtain an image of the epithelial surface, an area of 60 × 60 μm^2 was scanned with the excitation light beam. In Figure 2*B*, the black-and-white image results from fluorescence intensity measurements and reveals the outlines of supporting cells but only a few dendritic knobs. In the color-coded 2P-FLIM image, $[Cl^-]_i$ is represented by a color scale, with warmer colors indicating higher $[Cl^-]_i$ levels. Dendritic knobs appear as prominent red blots on a green background of supporting cells. Cilia are not visible on these images. The water-filled volume of rat olfactory cilia is estimated to be 3×10^{-18} l/μm length (Lindemann, 2001), accommodating $<10^4$ MQAE molecules at an intracellular MQAE concentration of 5 mM, which is not sufficient to allow fluorescence detection with our optical system. Thus, we visualized the dendritic knobs at the epithelial surface, which are more or less spherical structures with a volume of $\sim 10^{-14}$ l. Electron microscopy studies

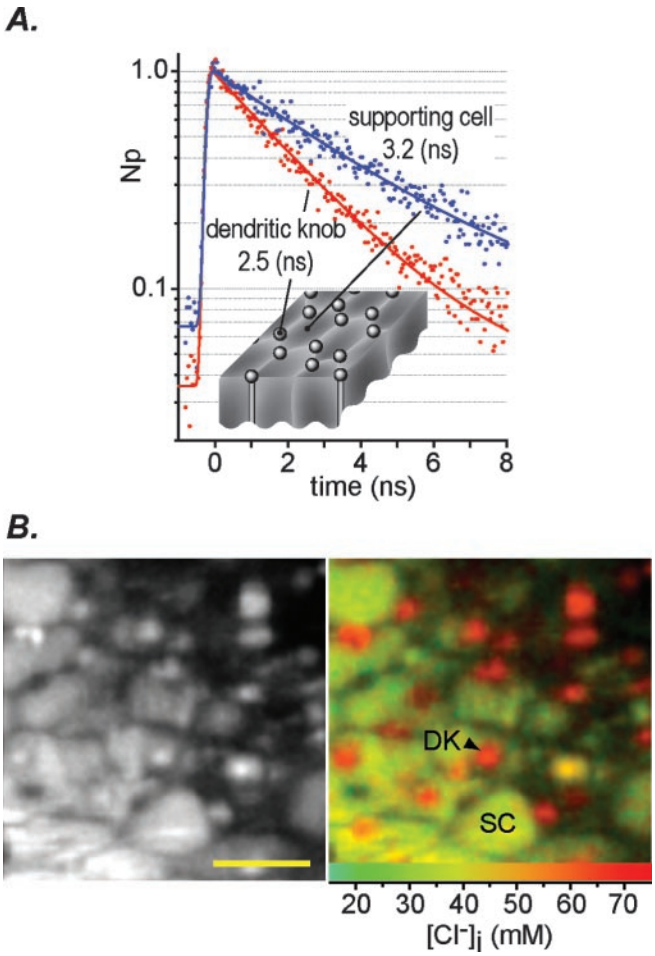

Figure 2. 2P-FLIM of the olfactory epithelium. *A*, 2P-FLIM recordings from MQAE-loaded olfactory epithelium yield different fluorescence lifetimes in dendritic knobs and supporting cells. The lower value measured in knobs indicates a higher intracellular Cl^- concentration compared with supporting cells. Np indicates the normalized number of photons analyzed for fluorescence lifetime. *B*, Fluorescence intensity image (left) and fluorescence lifetime image (right) of the same area of mouse olfactory epithelium loaded with MQAE. The outlines of supporting cells (SC) can be seen in both images. Dendritic knobs (DK), however, can be more easily discerned in the false-color 2P-FLIM representation where warmer colors indicate higher levels of $[Cl^-]_i$. In the top right corner, the epithelial surface retreats below the focal plane, and only the protruding dendritic knobs remain visible. Scale bar, 10 μm.

(Menco, 1997) and patch-clamp measurements (Lowe and Gold, 1991) have indicated that there is no diffusional barrier between cilia and dendritic knobs. Therefore, we assume that, under steady-state conditions, $[Cl^-]_i$ in dendritic knobs and ciliary lumen are similar.

Steady-state $[Cl^-]_i$ in dendritic knobs

To obtain absolute values for $[Cl^-]_i$, 2P-FLIM signals were calibrated with known $[Cl^-]_i$ values. $[Cl^-]_i$ was set to one of four levels (30, 45, 60, or 90 mM) by exposing the epithelium to a solution containing the required Cl^- concentration (Cl^- standard solutions) (Table 1) as well as 10 μM tributyltin (a Cl^-–OH^- exchanger) and 10 μM nigericin (a K^+–H^+ exchanger). The combination of these ionophores has been shown to dissipate Cl^- gradients across the plasma membrane (Chao et al., 1989). Fluorescence lifetimes decreased from 3.5 to 2.2 nsec when $[Cl^-]_i$ was raised from 30 to 90 mM within the dendritic knobs (Fig. 3*A*). A Stern–Volmer plot of the calibration data (Fig. 3*B*) yielded quenching constants of 13 M^{-1} in mouse and 18 M^{-1} in

Table 1. Solutions (in millimolar concentration)

	Na^+	$NMDG^+$	K^+	Ca^{2+}	Mg^{2+}	Cl^-	$Gluconate^-$	SO_4^{2-}	MS^-	NO_3^-
Extracellular solution	140		5	2	1	151				
50 Cl^- extracellular solution	140		5	2	1	50.3	99.3	0.7		
0 Na^+ extracellular solution		140	5	2	1	151				
0 Na^+–50 Cl^- extracellular solution		140	5	2	1	50.3	6	0.7	93.3	
Cell isolation solution	140		5			145				
30 Cl^- standard solution			150			30				120
45 Cl^- standard solution			150			45				105
60 Cl^- standard solution			150			60				90
90 Cl^- standard solution			150			90				60

Solutions contained 10 mM glucose; pH 7.4 was buffered with HEPES. The cell isolation solution was buffered with phosphate (in mM: 1.9 NaH_2PO_4, 8.1 Na_2HPO_4). MS^-, Methane sulfonate; NMDG, *N*-methyl-D-glucamine.

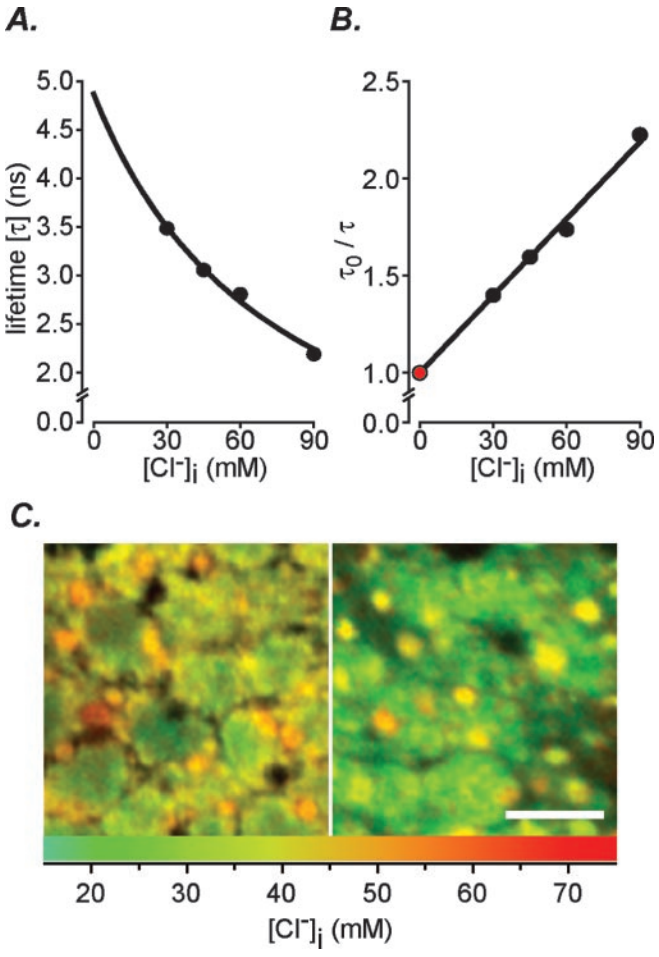

Figure 3. Determination of $[Cl^-]_i$ in dendritic knobs. *A*, Dependence of fluorescence lifetimes in mouse olfactory epithelium on $[Cl^-]_i$. *B*, Determination of the Stern–Volmer constant (13 M^{-1}) for MQAE in the tissue. Lifetime at 0 mM Cl^- (τ_0) was calculated from the curve in *A*. The data were obtained from a tissue preparation in which $[Cl^-]_i$ of OSNs and supporting cells was set to the indicated values using Cl^- ionophores and the standard solutions listed in Table 1. *C*, $[Cl^-]_i$ in dendritic knobs of rat (left) and mouse (right) olfactory epithelium at an extracellular $[Cl^-]$ of 50 mM, corresponding to the mucosal $[Cl^-]$ *in vivo*. Mean values are 54 ± 4 mM in rat (96 knobs) and 37 ± 6 mM in mouse (406 knobs). Scale bar, 10 μm.

rat, which were used in all of the additional experiments to calculate $[Cl^-]_i$ from the measured lifetimes. Steady-state $[Cl^-]_i$ in dendritic knobs was measured in a bath solution containing 50 mM Cl^- (Table 1), a value close to the mucosal Cl^- concentration reported for rat olfactory epithelium (Reuter et al., 1998). The mean $[Cl^-]_i$ in knobs of rat OSNs under these conditions was 54 ± 4 mM (96 knobs in eight epithelia) (Fig. 3*C*, left). $[Cl^-]_i$ values in dendritic knobs of mouse OSNs were somewhat lower, with a mean of 37 ± 7 mM (406 knobs in 18 epithelia) (Fig. 3*C*, right). We never observed dendritic knobs whose $[Cl^-]_i$ would be consistent with either passive distribution of Cl^- or with Cl^- extrusion ($[Cl^-]_i < 10$ mM). These results demonstrate that rat and mouse OSNs actively accumulate Cl^- in their dendritic endings against an electrochemical gradient. With approximately equal Cl^- concentrations on both sides of the ciliary plasma membrane, the Cl^- equilibrium potential E_{Cl} is close to 0 mV, and indicates a strong driving force for Cl^- efflux at negative membrane voltages.

The site of Cl^- uptake

Cl^- accumulation in the dendritic knobs may take either of two cellular paths: via the basolateral membrane or through the apical membrane. It is particularly important to localize the site of Cl^- uptake, because the ion composition of the mucus is unlike that of the standard interstitial solution, in that it contains less Na^+ and Cl^- but more K^+ (Reuter et al., 1998). Ion gradients that determine currents through channels and ion fluxes through transporters and exchangers in the ciliary membrane are, consequently, different from those at the basolateral membrane of OSNs. We reasoned that the site of Cl^- entry might be revealed at elevated extracellular Cl^- concentration. $[Cl^-]_i$ should rise fastest near the entry site, and a steady concentration profile along the dendrite–cilia axis should indicate the site of Cl^- influx. To look for such a profile, we measured $[Cl^-]_i$ in optical sections at 2 μm intervals, starting from the top of the dendritic knobs and extending ~10 μm deep into the epithelium (Fig. 4*A*). With 50 mM extracellular Cl^-, the $[Cl^-]_i$ profile along the dendrite was constant at ~55 mM (Fig. 4*B*, blue trace). In tissue samples that were continuously held at 150 mM Cl^-, we observed a standing $[Cl^-]_i$ gradient within the distal dendrites that ranged from 69 ± 7 mM (11 knobs) at the dendritic knobs to 57 ± 3 mM (7 knobs) 10 μm below the tissue surface (Fig. 4*B*, red trace). The gradient did not change during the observation time of 20–40 min, suggesting persistent Cl^- influx at the apical end of the dendrites. This result indicates that the apical membrane of OSNs is a site of Cl^- entry. Transport molecules involved in Cl^- homeostasis appear to be localized in the ciliary membrane, and the ion concentrations in the olfactory mucus are, therefore, relevant for Cl^- accumulation. The occurrence of the standing Cl^- gradient suggests that basolateral Cl^- uptake is much less efficient than uptake through the apical membrane.

Cl^- uptake mechanisms in intact OSNs

Cl^- accumulation against an electrochemical gradient must be linked to an energy source, either to the gradient of another ion or to the hydrolysis of ATP. Probably best understood is Cl^- accumulation in epithelial cells mediated by Na–K–2Cl cotransporters (Russell, 2000). This transporter uses the inward Na^+ gradi-

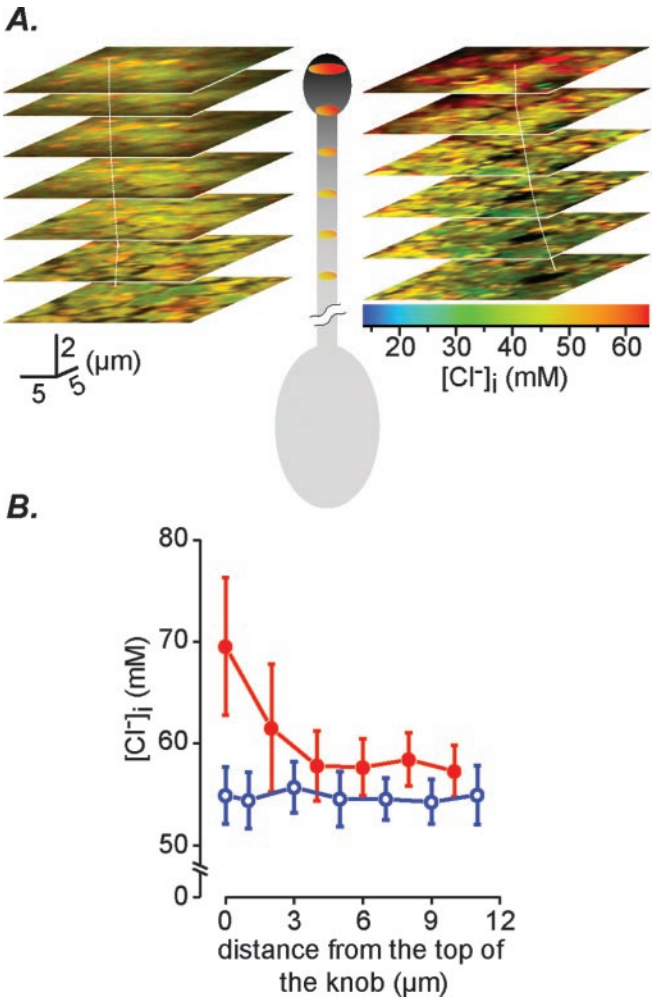

Figure 4. The site of Cl^- uptake. *A*, Optical sectioning by 2P-FLIM extending from the surface of rat olfactory epithelium 10 μm deep into the tissue, recorded with either 50 mM (left stack) or 150 mM (right stack) extracellular Cl^-. The white lines follow dendrites through the 2 μm intervals. An increase in $[Cl^-]_i$ occurs near the apical end of the dendrites in 150 mM extracellular Cl^-. *B*, Axial $[Cl^-]_i$ profiles in dendrites near the apical surface. With 50 mM extracellular Cl^-, $[Cl^-]_i$ was near 55 mM and no Cl^- gradient was established (blue line). At 150 mM extracellular Cl^- (red line), a standing $[Cl^-]_i$ gradient formed between the knobs (70 mM) and the proximal dendrite (55 mM), suggesting that Cl^- enters OSNs via the cilia. Means ± SD (7–14 knobs per point).

ent to drive an uphill Cl^- transport into the cell. Transport activity is electrically neutral and, hence, does not depend on membrane voltage. Moreover, it can be identified by its sensitivity to micromolar concentrations of the diuretic bumetanide. To test for an involvement of Na–K–2Cl cotransporters in Cl^- accumulation in OSNs, we monitored $[Cl^-]_i$ in dendritic knobs while changing extracellular Cl^- from 150 to 50 mM and back to 150 mM at intervals of 15 min. Under control conditions, this protocol caused $[Cl^-]_i$ to decrease by ~10 mM, followed by full recovery in 150 mM extracellular Cl^- (Fig. 5*A*;*B*, top trace). The recovery of $[Cl^-]_i$ is a consequence of Cl^- accumulation, and this process was completely blocked by 50 μM bumetanide (Fig. 5*B*, middle trace). Because Na–K–2Cl cotransport depends on the presence of extracellular Na^+, we repeated the experiment in a solution in which Na^+ was replaced by the impermeable cation $NMDG^+$ (Table 1) (0 mM Na^+ extracellular solution). Recovery of $[Cl^-]_i$ in 150 mM extracellular Cl^- was prevented in Na^+-free solution, and only occurred after the control Na^+ concentration was restored (Fig. 5*B*, bottom trace). The observation of a Na^+-dependent, bumetanide-sensitive Cl^- uptake into dendritic knobs is consistent with the activity of a Na–K–2Cl cotransporter.

To identify by PCR the isoform of Na–K–2Cl cotransporter as well as other Cl^- transporters present in OSNs, we designed primers for the Na–K–2Cl cotransporters NKCC1 and NKCC2, for the K–Cl cotransporters KCC1 and KCC2, and for the bumetanide-resistant cotransporter NCC (thiazide-sensitive Na–Cl cotransporter) (Gamba et al., 1994). Primers were designed to distinguish between transporter subtypes and to span several exons of the respective gene (see Materials and Methods). PCR experiments on rat olfactory epithelium cDNA showed that mRNA for NKCC1, NCC, and KCC1 is expressed, but no signal could be detected for NKCC2 and KCC2 (Fig. 5*C*). Positive controls were kidney cDNA for NKCC1, NKCC2, and NCC (Gamba et al., 1994; Lytle et al., 1995), cerebellum cDNA for KCC1 (Kanaka et al., 2001), and hippocampus cDNA for KCC2 (Kanaka et al., 2001). This result suggests that NKCC1 supplies the Cl^- uptake mechanism that we detected functionally using 2P-FLIM. Of particular interest is the absence of KCC2 expression, because this protein provides the main contribution to keeping $[Cl^-]_i$ low in CNS neurons (Rivera et al., 1999; Stein et al., 2004) (see Discussion). The lack of KCC2 expression is indicative of ion homeostasis designed to support elevated levels of $[Cl^-]_i$.

Impaired Cl^- accumulation in isolated OSNs

Most physiological data on OSNs result from experiments with cells isolated from the olfactory epithelium. Because Cl^- ions carry the largest part of the receptor current in rodent OSNs, a functional Cl^- accumulation mechanism is essential for the odor response also in isolated cells. 2P-FLIM measurements in 150 mM extracellular Cl^- revealed that $[Cl^-]_i$ is 30 ± 8 mM (100 cells from 15 rats) (Fig. 6*A*;*B*, blue histogram) in dendritic knobs of isolated OSNs, whereas OSNs in the intact epithelium had a mean $[Cl^-]_i$ of 62 ± 6 mM (39 cells) in the same solution (150 mM extracellular Cl^-) (Fig. 6*B*, red histogram). Less than 10% of isolated cells displayed a level of $[Cl^-]_i$ in the dendritic knob that was comparable with OSNs in intact tissue, and only these cells can be expected to respond to stimulation with a significant Cl^- contribution to the receptor current. This result is in agreement with a previous study of $[Cl^-]_i$ in isolated rat OSNs (Kaneko et al., 2001). In that report, OSNs were selected for their ability to accumulate Cl^- over 30 mM. The mean $[Cl^-]_i$ in the knobs of these cells was 81 mM (SD, 43 mM; 10 cells), which corresponds to the small fraction of isolated OSNs found to maintain elevated $[Cl^-]_i$ in the present study.

Discussion

The olfactory neuroepithelium presents specific challenges for physiological investigations, because the primary transduction processes occur within structures that are not easily accessible by conventional methods of experimentation. In mammals, sensory cilia are membrane tubes of ~10 μm length with a diameter of <200 nm (Menco, 1997). Moreover, these tiny tubes are immersed in mucus, an extracellular medium of mostly unknown composition that determines ion fluxes and response characteristics of OSNs *in vivo*. Despite a wealth of information on olfactory signal transduction resulting from biochemical, biophysical, and molecular studies (Schild and Restrepo, 1998; Buck, 2000; Frings, 2001; Paysan and Breer, 2001), some basic questions about how OSNs respond to stimulation remain unanswered. Prominent among these is the question about the amplitude, the time course, and the ionic composition of the receptor current *in*

vivo, a question that has stimulated considerable interest, because unlike other sensory neurons, OSNs employ two different types of transduction channels. After the discovery of Ca^{2+}-activated Cl^- channels in the ciliary membrane of frog OSNs (Kleene and Gesteland, 1991), the concept was soon developed that these channels may serve to amplify the receptor current (Kleene, 1993; Kurahashi and Yau, 1993; Lowe and Gold, 1993) and to enhance the detection efficiency of the olfactory system. The precondition for such an unusual amplification mechanism is, however, an outward-directed driving force for Cl^- ions that supports a depolarizing Cl^- efflux from the cilia into the mucus. This requires active Cl^- accumulation into the ciliary lumen, a process that has hitherto not been demonstrated.

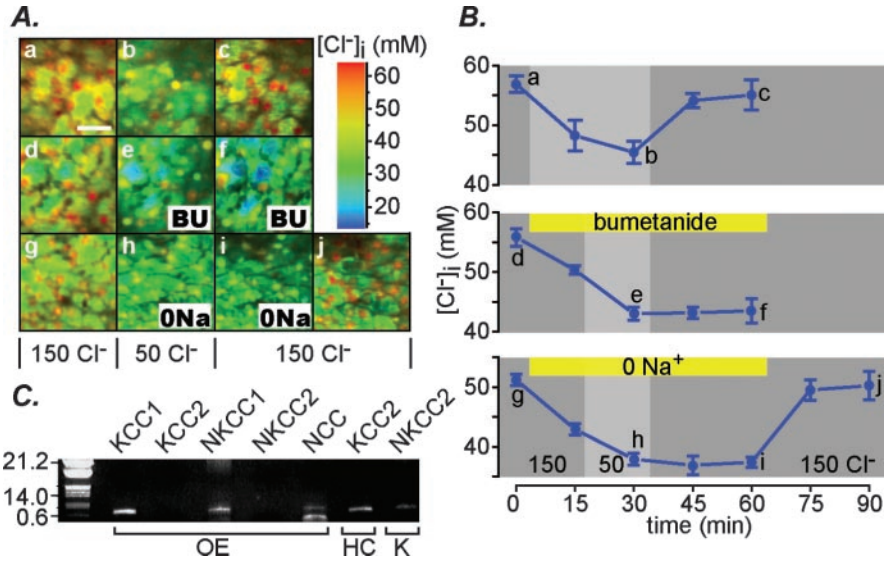

Figure 5. Cl^- uptake mechanisms in mouse OSNs. *A*, 2P-FLIM images of the epithelial surface during transient exposure to 50 mM extracellular Cl^-. $[Cl^-]_i$ in dendritic knobs declined when extracellular Cl^- was reduced from 150 to 50 mM and recovered after high Cl^- was restored (*a–c*). Bumetanide (BU) (50 μM) prevented recovery (*d–f*) as did exposure to Na^+-free solution (*g–j*). Scale bar, 10 μm. *B*, Quantitative analysis of $[Cl^-]_i$ of the experiment shown in *A*. The light gray area indicates the time interval when extracellular Cl^- was reduced from 150 to 50 mM. Reuptake of Cl^- into the dendritic knobs was suppressed by bumetanide and by exposure to Na^+-free solution. Na^+-dependent, bumetanide-sensitive Cl^- uptake represents evidence for the activity of a NKCC-type Cl^- transporter. Mean ± SEM of five to eight knobs. *C*, Detection of Cl^- transporter mRNA in rat olfactory epithelium. RT-PCR experiments yielded signals for KCC1, NKCC1, and NCC in olfactory epithelium cDNA (OE). No expression of KCC2 or NKCC2 was detected. Positive controls for KCC2 [rat hippocampus (HC)] and for NKCC2 [rat kidney (K)] are shown on the right.

Cl^- accumulation in olfactory cilia

If a neuron actively accumulates Cl^-, E_{Cl} becomes more positive than the resting membrane voltage, and the opening of Cl^- channels leads to Cl^- efflux and depolarization. The first evidence for Cl^- accumulation in OSNs came from patch-clamp studies of isolated amphibian OSNs (Dubin and Dionne, 1994; Zhainazarov and Ache, 1995), in which about one-half of the receptor current can be carried by Cl^- (Kleene, 1997). For rodents, a first estimate for $[Cl^-]_i$ inside the dendritic knobs was obtained by a combination of energy-dispersive x-ray microanalysis (EDXA) and electron-scattering analysis applied to cryosections of rat olfactory epithelium (Reuter et al., 1998). A mean value of 69 mM Cl^- was obtained in that study and indicated efficient Cl^- accumulation. The result obtained in the present 2P-FLIM study of living OSNs in intact olfactory epithelium (mean $[Cl^-]_i$, 54 mM when extracellular Cl^- was 50 mM) is in fair agreement with the results by Reuter et al. (1998) and strongly supports the hypothesis that OSNs sustain an elevated level of $[Cl^-]_i$ *in vivo*.

The uptake mechanism resides in the apical membrane, most probably within the ciliary membrane or in the membrane of the dendritic knobs. The source for Cl^- is the olfactory mucus, and the driving force for Cl^-–cation cotransport results from the respective ion gradients across the apical, chemosensory membrane. NKCC1 cotransporters in the apical membrane couple Cl^- uptake to inward Na^+ flux, and the absence of KCC2 fits the picture of a neuron designed for Cl^- accumulation. The K–Cl cotransporter KCC2 is expressed in neurons of the mammalian CNS after birth, a process that causes the "chloride switch," the transition from excitatory Cl^- currents in the embryonic CNS to inhibitory Cl^- currents in the adult CNS (Rivera et al., 1999; Hubner et al., 2001; Stein et al., 2004). KCC2 couples Cl^- efflux to the outward K^+ gradient in the adult CNS, and the continuous Cl^- extrusion decreases neuronal $[Cl^-]_i$ to levels of <10 mM (Kaila, 1994). Only a few types of neurons seem to lack this chloride switch. Somatosensory neurons of the dorsal root ganglia do not express KCC2 and, consequently, uphold an elevated level of $[Cl^-]_i$ during adult life (Rivera et al., 1999). 2P-FLIM measurements revealed a mean $[Cl^-]_i$ of 31 mM (Kaneko et al., 2002), which probably results from the activity of Na–K–2Cl cotransporters (Sung et al., 2000; Alvarez-Leefmans et al., 2001), and explains that these neurons depolarize when challenged with GABA (Duchen, 1990). In mammalian OSNs, Cl^- homeostasis seems to be organized along similar lines.

A role for NKCC1 in olfactory signal transduction

The driving force for passive Cl^- uptake by NKCC1 can be assessed from the EDXA analysis of rat olfactory mucus, which yielded the first estimates for mucosal ion concentrations *in vivo* (in mM): 55 ± 12 Na^+, 69 ± 10 K^+, and 55 ± 11 Cl^- (Reuter et al., 1998). Intracellular ion concentrations are 172 ± 23 mM for K^+ (Reuter et al., 1998) and 54 ± 4 mM for Cl^- (this study). $[Na^+]_i$ could not be determined with sufficient accuracy by EDXA (53 ± 31 mM) (Reuter et al., 1998). These concentrations result from the activity of various transport proteins and ion channels in the cilia and can be used to derive the minimal Na^+ gradient across the ciliary membrane necessary to support the elevated level of $[Cl^-]_i$. Calculating the driving force for Na–K–2Cl cotransport according to the following:

$$\Delta G = RT \times \ln \frac{[Na]_i[K]_i[Cl]_i^2}{[Na]_o[K]_o[Cl]_o^2}$$

shows that equilibrium ($\Delta G = 0$; no Cl^- uptake) is achieved at $[Na^+]_i = 23$ mM. Consequently, the NKCC1 cotransporter contributes to Cl^- accumulation only if $[Na^+]_i$ is <23 mM, or if $[Cl^-]_i$ drops below the measured steady-state value of 54 mM. At higher values of $[Na^+]_i$ or $[Cl^-]_i$, the cotransporter extrudes Cl^- into the mucus. Thus, NKCC1 counteracts a decrease of $[Cl^-]_i$ in the cilia below its resting level of 54 mM, buffering against excessive loss of ciliary Cl^- during odor stimulation. In fact, the activation of Ca^{2+}-gated Cl^- channels in the ciliary membrane

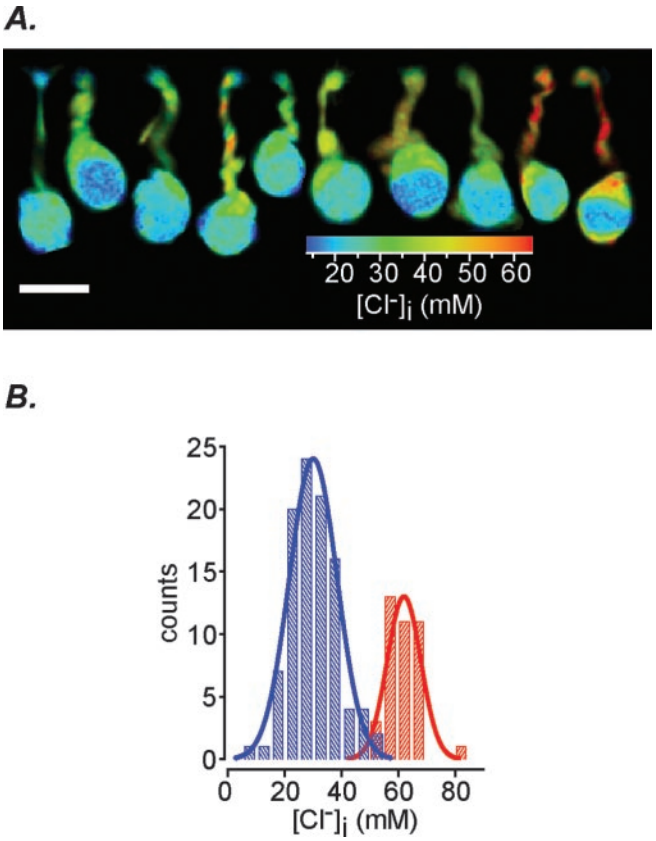

Figure 6. Impaired Cl^- homeostasis in isolated OSNs. *A*, 2P-FLIM images from isolated rat OSNs loaded with MQAE, sorted by the $[Cl^-]_i$ in their dendritic knobs. $[Cl^-]_i$ ranges from 20 to 60 mM. The extracellular Cl^- concentration was 150 mM. Scale bar, 10 μm. *B*, Distribution of $[Cl^-]_i$ values in dendritic knobs of isolated OSNs (blue histogram; 30 ± 8 mM; 100 cells) and in knobs in intact epithelium (red histogram; 62 ± 6 mM; 39 cells) in the presence of 150 mM extracellular Cl^-. Most isolated OSNs showed a reduced ability to accumulate Cl^-.

would rapidly deplete the ciliary lumen of Cl^- (Lindemann, 2001). To generate multiple or prolonged responses, OSNs require a mechanism that efficiently replenishes ciliary $[Cl^-]_i$. NKCC1 mediates this Cl^- uptake and acts to stabilize $[Cl^-]_i$ within the ciliary lumen. The cotransporter thereby contributes to maintaining the electrical responsiveness of the OSN.

Impaired Cl^- homeostasis in isolated OSNs

Our finding that most isolated rat OSNs lose their ability to accumulate intracellular Cl^- represents a serious caveat for the interpretation of functional data obtained from such cells. More than 80% of the receptor current in intact mammalian OSNs is carried by Cl^- ions (Lowe and Gold, 1993; Reisert et al., 2003), and a loss of this current fraction must be expected to compromise the response of the cell to odor stimulation. A lack of response in isolated OSNs may, therefore, either indicate absence of the appropriate subtype of odorant receptor or, alternatively, the inability of the cell to generate a receptor current of sufficient amplitude. The interpretation of negative results from isolated OSNs is, therefore, unreliable. Especially in experiments with intact, isolated cells (Ca^{2+} imaging, suction electrode), the residual level of $[Cl^-]_i$ may be too low to support the expected sensory response. Whole-cell recordings overcome this problem by supplying Cl^- through the pipette solution, thus providing a constant level of $[Cl^-]_i$ in the cilia even when Cl^- uptake mechanisms are no longer active. What is the reason for the failure of Cl^- accumulation in most isolated OSNs? One reason could be the loss of cilia, and hence Cl^- transporters, during isolation. Furthermore, redistribution of ciliary membrane proteins may follow opening of the tight junctions during the isolation process (Pisam and Ripoche, 1976). If the NKCC1 proteins are no longer concentrated in the cilia but distributed over the entire cell surface, their local density may not be sufficient to maintain high $[Cl^-]_i$ levels in the bulk cytosol. Thus, the Cl^- accumulation mechanism of OSNs appears to be designed to support Cl^- homeostasis only inside the small lumen of the sensory cilia.

Our results show that mammalian OSNs accumulate intracellular Cl^- within the lumen of their sensory cilia, where Cl^- is needed as charge carrier for the receptor current. OSNs are the only sensory neurons in direct contact with the external environment, and originally, the Cl^--based receptor current was interpreted as a means of sustaining sensory function under conditions of changing ion concentrations at the ciliary tissue surface (Kleene and Pun, 1996). Particularly in freshwater fish and amphibia, intracellular Cl^- may be a more reliable ion source for generating receptor currents than external cations. Although this notion is consistent with olfactory function in aquatic animals, it does not necessarily apply to mammals in which the olfactory mucosa is shielded from contact with water. Moreover, the mucosal ion composition of the mucus can be regulated by mucus glands that are themselves controlled by the autonomic nervous system (Getchell et al., 1988). Cl^- uptake into OSNs is more likely an example of a specific strategy for the control of excitability that also operates in other neurons. Elevated levels of $[Cl^-]_i$ give rise to depolarizing Cl^- efflux in the embryonic CNS, but also in various populations of adult neurons, including retinal bipolar cells (Billups and Attwell, 2002), somatosensory neurons (Kaneko et al., 2002), and the neurons of the suprachiasmatic nucleus where $[Cl^-]_i$ appears to oscillate at a circadian rhythm (Wagner et al., 2001; Shimura et al., 2002). 2P-FLIM of MQAE fluorescence is a suitable technique to study these phenomena quantitatively in living cells.

References

Alvarez-Leefmans FJ, Leon-Olea M, Mendoza-Sotelo J, Alvarez FJ, Anton B, Garduno R (2001) Immunolocalization of the Na^+-K^+-$2Cl^-$ cotransporter in peripheral nervous tissue of vertebrates. Neuroscience 104:569–582.

Billups D, Attwell D (2002) Control of intracellular chloride concentration and GABA response polarity in rat retinal ON bipolar cells. J Physiol (Lond) 545:183–198.

Buck LB (2000) The molecular architecture of odor and pheromone sensing in mammals. Cell 100:611–618.

Chao AC, Dix JA, Sellers MC, Verkman AS (1989) Fluorescence measurement of chloride transport in monolayer cultured cells. Mechanisms of chloride transport in fibroblasts. Biophys J 56:1071–1081.

Denk W, Svoboda K (1997) Photon upmanship: why multiphoton imaging is more than a gimmick. Neuron 18:351–357.

Dubin AE, Dionne VE (1994) Action potentials and chemosensitive conductances in the dendrites of olfactory neurons suggest new features for odor transduction. J Gen Physiol 103:181–201.

Duchen MR (1990) Effects of metabolic inhibition on the membrane properties of isolated mouse primary sensory neurones. J Physiol (Lond) 424:387–409.

Dzeja C, Hagen V, Kaupp UB, Frings S (1999) Ca^{2+} permeation in cyclic nucleotide-gated channels. EMBO J 18:131–144.

Frings S (2001) Chemoelectrical signal transduction in olfactory sensory neurons of air-breathing vertebrates. Cell Mol Life Sci 58:510–519.

Gamba G, Miyanoshita A, Lombardi M, Lytton J, Lee WS, Hediger MA, Hebert SC (1994) Molecular cloning, primary structure, and characterization of two members of the mammalian electroneutral sodium-(potassium)-chloride cotransporter family expressed in kidney. J Biol Chem 269:17713–17722.

Getchell ML, Zielinski B, Getchell TV (1988) Odorant and autonomic reg-

ulation of secretion in the olfactory mucosa. In: Molecular neurobiology of the olfactory system (Margolis FL, Getchell TV, eds), pp 71–98. New York: Plenum.

Getchell TV, Margolis FL, Getchell ML (1984) Perireceptor and receptor events in vertebrate olfaction. Prog Neurobiol 23:317–345.

Hubner CA, Stein V, Hermans-Borgmeyer I, Meyer T, Ballanyi K, Jentsch TJ (2001) Disruption of KCC2 reveals an essential role of K-Cl cotransport already in early synaptic inhibition. Neuron 30:515–524.

Kaila K (1994) Ionic basis of GABAA receptor channel function in the nervous system. Prog Neurobiol 42:489–537.

Kanaka C, Ohno K, Okabe A, Kuriyama K, Itoh T, Fukuda A, Sato K (2001) The differential expression patterns of messenger RNAs encoding K-Cl cotransporters (KCC1,2) and Na-K-2Cl cotransporter (NKCC1) in the rat nervous system. Neuroscience 104:933–946.

Kaneko H, Nakamura T, Lindemann B (2001) Noninvasive measurement of chloride concentration in rat olfactory receptor cells with use of a fluorescent dye. Am J Physiol 280:C1387–C1393.

Kaneko H, Putzier I, Frings S, Gensch T (2002) Determination of intracellular chloride concentration in dorsal root ganglion neurons by fluorescence lifetime imaging. In: Calcium-activated chloride channels (Fuller CM, ed), pp 167–189. Boston: Academic.

Kleene SJ (1993) Origin of the chloride current in olfactory transduction. Neuron 11:123–132.

Kleene SJ (1997) High-gain, low-noise amplification in olfactory transduction. Biophys J 73:1110–1117.

Kleene SJ, Gesteland RC (1991) Calcium-activated chloride conductance in frog olfactory cilia. J Neurosci 11:3624–3629.

Kleene SJ, Pun RYL (1996) Persistence of the olfactory receptor current in a wide variety of extracellular environments. J Neurophysiol 75:1386–1390.

Koncz C, Daugirdas JT (1994) Use of MQAE for measurements of intracellular $[Cl^-]$ in cultured aortic smooth muscle cells. Am J Physiol 267:H2114–H2123.

Kurahashi T, Yau KW (1993) Co-existence of cationic and chloride components in odorant-induced current of vertebrate olfactory receptor cells. Nature 363:71–74.

Lakowicz JR (1999) Principles of fluorescence spectroscopy, Ed 2. New York, London: Kluwer Academic/Plenum.

Leinders-Zufall T, Greer CA, Shepherd GM, Zufall F (1998) Imaging odor-induced calcium transients in single olfactory cilia: specificity of activation and role in transduction. J Neurosci 18:5630–5639.

Li JH, Lindemann B (2003) Multi-photon microscopy of cell types in the viable taste disk of the frog. Cell Tissue Res 313:11–27.

Lindemann B (2001) Predicted profiles of ion concentrations in olfactory cilia in the steady state. Biophys J 80:1712–1721.

Lowe G, Gold GH (1991) The spatial distributions of odorant sensitivity and odorant-induced currents in salamander olfactory receptor cells. J Physiol (Lond) 442:147–168.

Lowe G, Gold GH (1993) Nonlinear amplification by calcium-dependent chloride channels in olfactory receptor cells. Nature 366:283–286.

Lytle C, Xu JC, Biemesderfer D, Forbush III B (1995) Distribution and diversity of Na-K-Cl cotransport proteins: a study with monoclonal antibodies. Am J Physiol 269:C1496–C1505.

Marandi N, Konnerth A, Garaschuk O (2002) Two-photon chloride imaging in neurons of brain slices. Pflugers Arch 445:357–365.

Menco BP (1997) Ultrastructural aspects of olfactory signaling. Chem Senses 22:295–311.

Paysan J, Breer H (2001) Molecular physiology of odor detection: current views. Pflugers Arch 441:579–586.

Pisam M, Ripoche P (1976) Redistribution of surface macromolecules in dissociated epithelial cells. J Cell Biol 71:907–920.

Reisert J, Bauer PJ, Yau KW, Frings S (2003) The Ca-activated Cl channel and its control in rat olfactory receptor neurons. J Gen Physiol 122:349–363.

Reuter D, Zierold K, Schroder WH, Frings S (1998) A depolarizing chloride current contributes to chemoelectrical transduction in olfactory sensory neurons *in situ*. J Neurosci 18:6623–6630.

Rivera C, Voipio J, Payne JA, Ruusuvuori E, Lahtinen H, Lamsa K, Pirvola U, Saarma M, Kaila K (1999) The K^+/Cl^- co-transporter KCC2 renders GABA hyperpolarizing during neuronal maturation. Nature 397:251–255.

Russell JM (2000) Sodium-potassium-chloride cotransport. Physiol Rev 80:211–276.

Schild D, Restrepo D (1998) Transduction mechanisms in vertebrate olfactory receptor cells. Physiol Rev 78:429–466.

Shimura M, Akaike N, Harata N (2002) Circadian rhythm in intracellular Cl^- activity of acutely dissociated neurons of suprachiasmatic nucleus. Am J Physiol 282:C366–C373.

Stein V, Hermans-Borgmeyer I, Jentsch TJ, Hubner CA (2004) Expression of the KCl cotransporter KCC2 parallels neuronal maturation and the emergence of low intracellular chloride. J Comp Neurol 468:57–64.

Sung KW, Kirby M, McDonald MP, Lovinger DM, Delpire E (2000) Abnormal $GABA_A$ receptor-mediated currents in dorsal root ganglion neurons isolated from Na–K–2Cl cotransporter null mice. J Neurosci 20:7531–7538.

Verkman AS (1990) Development and biological applications of chloride-sensitive fluorescent indicators. Am J Physiol 259:C375–C388.

Wagner S, Sagiv N, Yarom Y (2001) GABA-induced current and circadian regulation of chloride in neurones of the rat suprachiasmatic nucleus. J Physiol (Lond) 537:853–869.

Zhainazarov AB, Ache BW (1995) Odor-induced currents in *Xenopus* olfactory receptor cells measured with perforated-patch recording. J Neurophysiol 74:479–483.